UNIVERSITY OF TARTU
Faculty of Science and Technology
Institute of Physics

Hendrik Ehrpais

ESTCUBE-1 IN-ORBIT ATTITUDE DETERMINATION VALIDATION

Bachelor's Thesis (12 ECTS)

Advisors:
M.Sc. Andris Slavinskis
B.Sc. Henri Kuuste

Tartu 2015

Contents

List of Tables

List of Figures

List of Acronyms

ADCS Attitude Determination and Control Subsystem

SVD singular value decomposition

TLE two-line element

SGP4 Simplified General Perturbation model

E-Sail Electric Solar Wind Sail

UKF unscented Kalman filter

IGRF 11 International Geomagnetic Reference Field 11

ADS attitude determination system

PSD position sensitive device

COTS commercial off the shelf

PSD position sensitive device

CAD computer-aided design

1 Introduction

ESTCube-1 is the first Estonian satellite launched to orbit on the 7th of May, 2013. One of the main missions of the satellite is to test the electric solar wind sail (E-Sail) propulsion concept invented by Pekka Janhunen from the Finnish Meterological institute. To test this concept a 10 meter long tether is deployed from the satellite using centrifugal force and the spin rate change caused by the Coulomb drag force is measured [3], [4].

The Attitude determination and Control System (ADCS) is the subsystem of ESTCube-1 that provides the required centrifugal force by spinning up the satellite to an angular velocity of one revolution per second while also keeping the spin axis parallel to the Earth's rotation axis [5]. The attitude determination system uses magnetometers, gyroscopes and sun sensors to determine the attitude of the satellite [2], [6].

After launching the satellite into orbit, a series of problems with sensors and the attitude determination process were encountered and corrected so the system could achieve the required attitude determination accuracy. Another goal was to improve the system's performance at higher angular velocities. The aim of the work presented in this Bachelor's thesis was to achieve functional attitude determination and to calibrate the system to estimate the attitude with an uncertainty below 2 degrees [2].

The main contributions of the author for this process in chronological order were (it should be noted that most of those contributions were made by the collaboration of the ADCS team and not by a single individual, but these I had a major part in):

- Developing the Sun sensors and developing filtering for the Sun sensor measurements in-orbit to make them provide the most optimal output for attitude determination.
- Validating and calibrating the angular velocity obtained from gyroscopes by comparing its results with the Sun vector results.
- Using the unscented Kalman filter UKF to estimate magnetometer biases that were the result of the residual magnetic moment of the satellite. These

biases were then removed during the filtering process.

- Temperature calibration of the gyroscopes and magnetometers.
- Improving the inertia matrix estimation by analysing the uncontrolled rotation of the satellite and comparing it to simulations. Implementing the full inertia matrix in the Kalman filter and attitude control instead of only the diagonal elements.
- Improving the model noise covariance matrix of the Kalman filter by running attitude determination with different covariance matrices. The results were then compared with image based attitude estimation to find the best match.
- Comparing the attitude estimation from the images with the attitude determination system to validate the attitude determination.

The flight results and system characterisation are also presented in an article, where I also contributed as a co-author, titled "Flight results of ESTCube-1 attitude determination system" in the Journal of Aerospace Engineering by A. Slavinskis, H. Ehrpais, H. Kuuste, et.al. [1]. The System design was described in a separate article, which I also co-authored, titled "Attitude determination and control for centrifugal tether deployment on the ESTCube-1 nanosatellite" by A. Slavisnkis, et.al [2]. There will also be an article about the attitude control system of ESTCube-1 written by the author of this thesis.

2 Nanosatellite attitude determination

Attitude determination uses a combination of sensors and mathematical models to estimate a satellite's attitude. First, the sensor data is converted into vectors that represent some physical object or property such as the Sun vector, Earth's magnetic field vector, star location vectors or other vectors that describe the attitude of the satellite. Then at least two reference vectors are required to estimate the attitude by solving Wahba's problem. The concept of the problem is to find a matrix that represents the rotation between the two coordinate systems represented by the measured vectors. The problem and different solutions are presented in various books and articles [7, p. 428], [8]. In our case the solution is based on the singular value decomposition (SVD) method. The implementation is based on the work of the AAUSAT team, who provided us with the initial software for attitude determination and simulations. The SVD method fails when the method lacks input from two independent sources. In our case this happens when the satellite is in eclipse or the system is unable to obtain the Sun or magnetic field vector. Because of this the attitude estimation is handled by the (UKF). It enables us to estimate the attitude based on the previous attitude results and the sensor data and isn't strictly dependent on having all of the inputs for every step. [8]

Nanosatellite attitude determination and control has been performed or planned by a number of satellites. Examples of satellites using different ADCSs are NanoSail-D [9], LightSail-1 [10], CubeSail [11], RAX [12], UniBRITE (CanX-3A) [13], TUGSAT-1/BRITE-Austria [14], SwissCube [15], AAUSAT-II [16], Firefly [17], Aalto-1 [18], MicroMAS [19] and CHIME [20], CanX-2 [21], CanX-4 and CanX-5 [22], COMPASS-1 [23] and STRaND-1 [24] ESTCube-1 is the first nanosatellite to perform high spin rate control using only electromagnetic actuators. A similar attitude determination and control system as on ESTCube-1 is also planned by Aalto-1, which also aims to test the E-sail concept.

2.1 ESTCube-1 attitude determination and control system design

The ESTCube-1 mission to measure the E-sail force required the attitude determination and control system to provide centrifugal force by rotating the satellite and measuring the spin rate change caused by the E-sail force [5]. The ADCS was required to spin up the satellite up to 360 $\text{deg}\cdot\text{s}^{-1}$and align its spin axis with the Earth's polar axis with a pointing error of less than 3°. This set the requirements on attitude determination accuracy, which should have an error of less than 2°. To spin up the satellite to these high angular velocities while aligning its axis with the Earth's polar axis, the attitude determination system (ADS) must be able to determine the attitude at those speeds. Magnetometers , gyroscopes and analogue Sun sensors were chosen for attitude determination, because these sensors are able to give an output at a high frequency and the data analysis doesn't take as long of a time as it would for Star trackers. The attitude control is handled by magnetic torquers because reaction wheels are unable to provide sufficient torque and have high power and mass requirements. At the time of designing the satellite there were also no suitable thrusters for nanosatellites. The sensors for attitude determination included 6 Sun sensors, 4 gyroscopes and 2 magnetometers. Temperature information is taken into account to correct magnetometer and gyroscope readings. The Design of the ESTCube-1 ADS is presented in Figure 1

The International Geomagnetic Reference Field 11 IGRF 11 is used for geomagnetic modeling [25]. Sun direction is calculated using the method described by Montenbruck and Pfleger [26, p. 39]. The orbit propagation model used is the Simplified General Perturbation model SGP4 [27]. The Earth rotation model is described in detail by the AAUSAT satellite team [8, p. 65]. The main consideration when choosing the models was to reduce the computational time for every attitude determination iteration.

2.2 Sun sensors

Because we did not find an existing adequate Sun sensor solution that would fit in the mass and energy budget for the satellite and the size was restricted by the

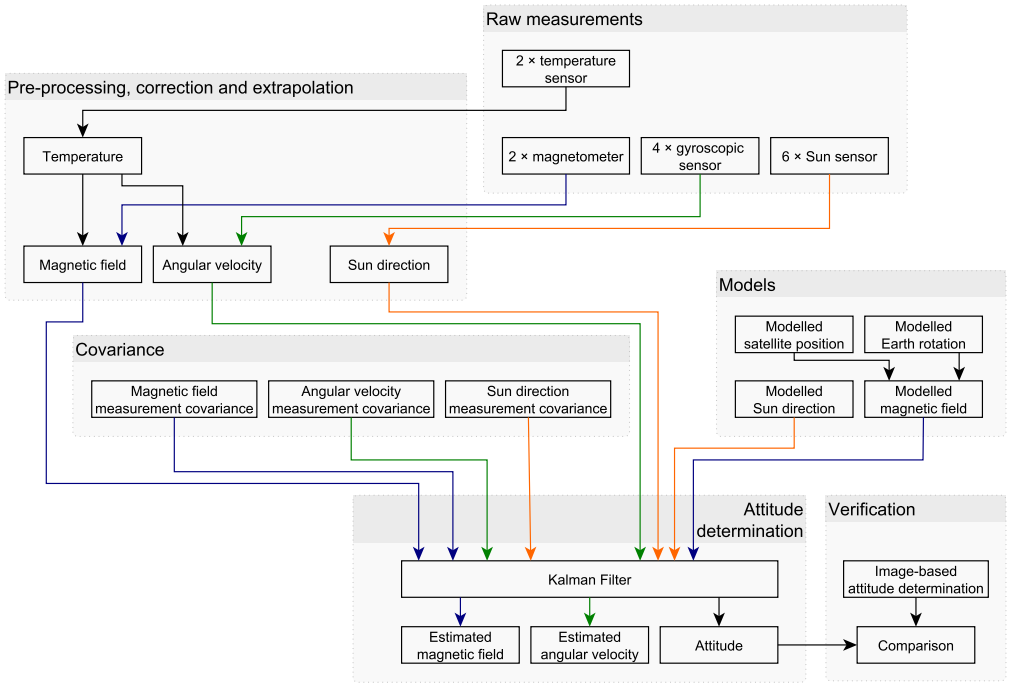

Figure 1: Data acquisition, processing and validation scheme of attitude determination system. [1]

structure of the satellite, the Sun sensors were custom developed by the ESTCube team. The Sun sensor hardware layout is presented in Figure 2. This shows a two-axis Sun sensor that uses two analogue Hamamatsu S3931 position sensitive devices (PSD) [28]. A light beam travels through the slit in the Sun sensor body and hits a part of the PSD. The PSD together with the electronics convert the light beam into two voltages that represent the location on the sensor. The voltages can be converted to the angle of incidence using the following equation [28].

$$\frac{I_2 - I_1}{I_1 + I_2} = \frac{2x}{L}$$

The expanded uncertainty for an angle of incidence was originally estimated at 2.5° [2], but because the calibration was unusable the estimation was not accurate. The methods on how the Sun sensor data is used are described under Chapter 3. Each sensor weighs 4.6 g and consumes 4 mW. Together with the analogue to digital converters the six sensors take up to 96 mW of power [2].

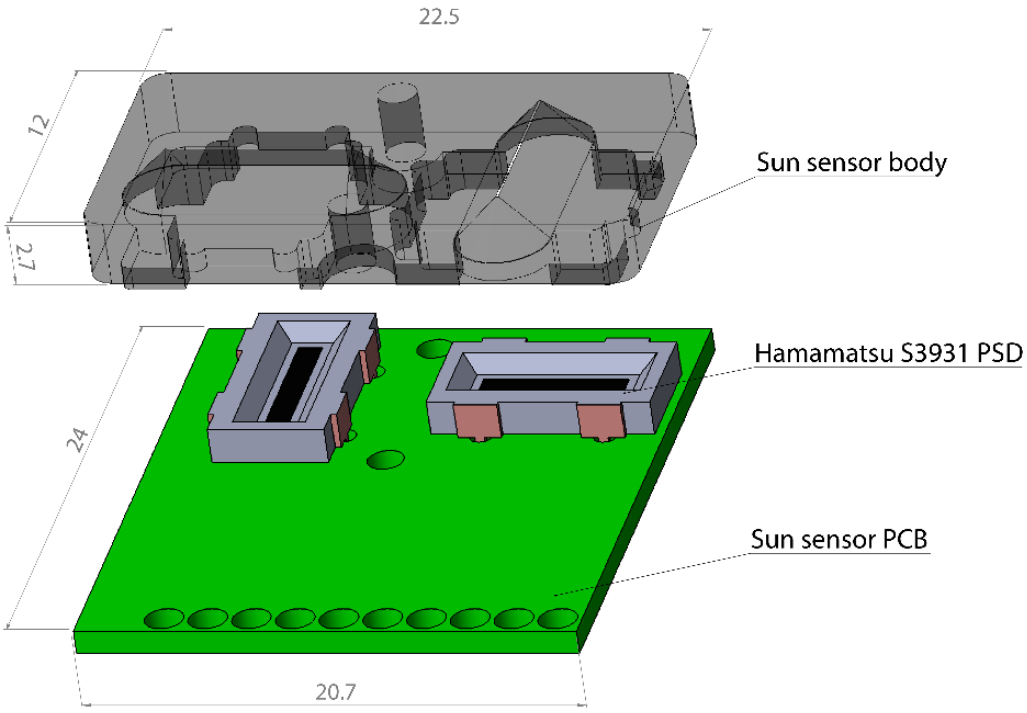

Figure 2: The Sun sensor hardware layout.[2]

2.3 Magnetometers

A commercial off-the-shelf (COTS) magnetometer was used for ESTCube-1. The chosen sensor was Honeywell HMC5883L [29], which utilises anisotropic magnetoresistive technology. This sensor is able to measure the direction of the local magnetic field. It was chosen because of its low mass(18 mg), low power consumtion(0.33mW), high sampling frequency(160 Hz) and acceptable resolution(60 nT) and range($\pm$0.13 mT) [2].

Because the magnetometers measure the local magnetic field, the residual magnetic moment of the satellite directly affects the results of the magnetometers. This effect had to be filtered out. The magnetometer bias estimation and temperature calibration are described in Chapter 3. The expanded uncertainty for the Earth's magnetic field was estimated at 3.2° [2], but because the sensors were recalibrated in orbit and the temperature influence mostly removed this is not an accurate uncertainty estimation. This uncertainty was however used for simulations and the uncertainty budget estimation.

2.4 Gyroscopes

The gyrocopic sensors used for ESTCube-1 were also COTS components. The sensor used was Invensense ITG-3200 [30]. It is based on the Coriolis effect and used to measure the angular velocity of the satellite.This sensor was selected because of its low mass (37 mg), low power consumption (21.5 mW), high sampling frequency (8200 Hz), sufficient resolution (0.07 deg·s^{-1}) and range ($\pm$2000 deg·s^{-1}) [2].

The estimated uncertainty for the gyroscopes was estimated at 3.6 deg·s^{-1}. This was mostly due to the temperature influence, which contributed 1.5 deg·s^{-1} (This is not expanded uncertainty). However, the temperature influence was compensated for and the offsets of the gyroscopes recalculated in-orbit. Because of this the gyroscopes achieved a significantly better performance than initially estimated. This process and results are described in Chapter 3.

2.5 Unscented Kalman filter

The UKF is a variant of the Kalman filter that is used when the predict and update functions are highly non-linear.The UKF is based on a sigma point sampling method called unscented transform that is used to pick a minimal set of sample points and to give an adequate coverage of the input and output probability distribution [8].

When the Kalman filter is first run the initial attitude is calculated using the SVD method, which uses the Sun and magnetic fields to calculate the attitude. Then the UKF uses the previous attitude to propagate a new attitude result. This is done in the following steps: 1) Calculate the sigma points using the error state covariance matrix. 2) Propagate all sigma points with the nonlinear system model and the input vector. 3) Calculate the a priori state estimate and the a priori error covariance matrix. 4) Predict measurements by propagating the sigma points through the sensor model to obtain the transformed sigma points. 5) Calculate the a posteriori state estimate using the measurement vector. 6) Calculate the a posteriori error covariance [31], [1].

The implementation of the Kalman filter uses the model noise covariance matrix and the measurement noise covariance matrix to estimate the biases of different sensors. These matrices are calibrated in-orbit by comparing the attitude estimations with different matrices to independent attitude determination that is based on images.

The predicition step is based on the Euler's rotation equations. Their general form is

$$\dot{\mathbf{I}} \cdot \dot{\boldsymbol{\omega}} + \boldsymbol{\omega} \times (\mathbf{I} \cdot \boldsymbol{\omega}) = \mathbf{M}.$$

where I is the inertia matrix, ω is the angular velocity vector and M is the applied torque.

2.6 Image-based attitude determination

To have an independent verification of the attitude determination system, image-based attitude determination was used. Images from Earth are taken by the on-board camera. The camera has a 4.4 mm telecentric lens and a 640 $\times$ 480 pixel sensor [32]. To estimate the attitude from a picture the coordinates from the images need to be matched up with corresponding coordinates in a geographic coordinate system. In Figure 3 a sample image is presented that shows how certain landmarks are distinguished and chosen on an image. The same points are then found in Google Earth and the coordinates are gathered. Then by minimizing the angular error between the two sets of vectors, an attitude vector that best represents the image is found. By using the time when the image was taken we are able to calculate the orbital position of the satellite using the SGP4 model and calculate the attitude of the spacecraft in the Earth-centered inertial reference frame. [27] The estimated attitude is then matched up with the sensor data that was taken at the same time in order to compare it with the ADS.

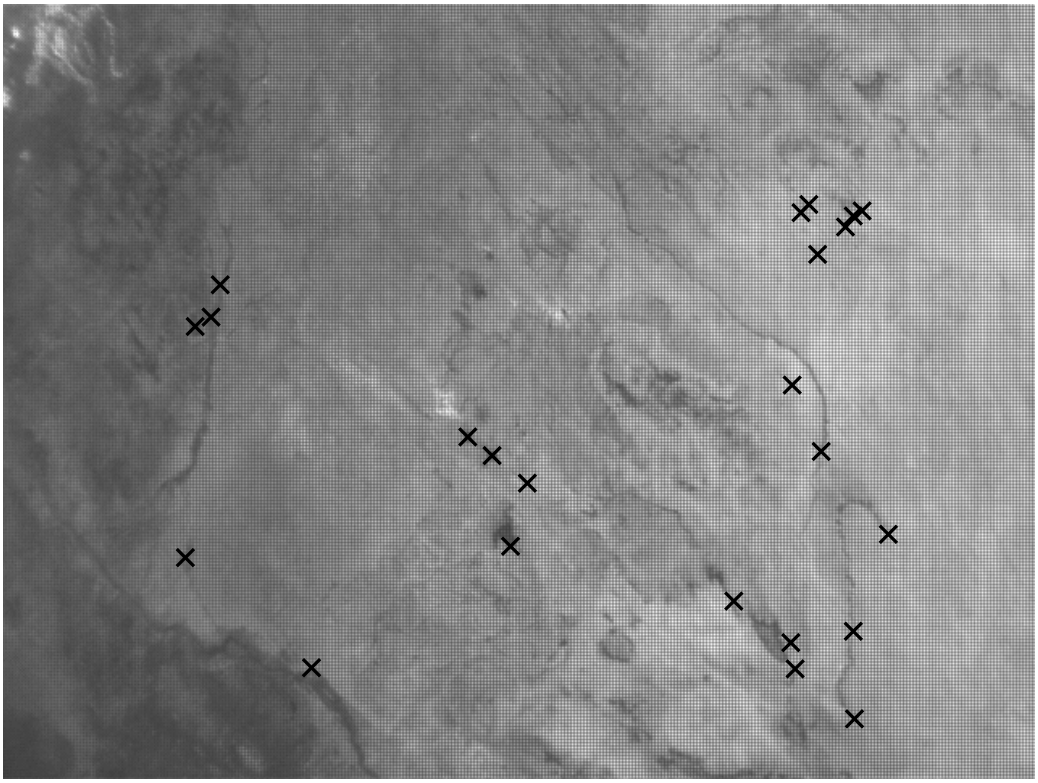

Figure 3: A typical image from ESTCube-1 with landmarks. [1]

3 In-orbit characterisation

After launching the satellite into orbit a number of problems were discovered with the attitude determination system. The sensors were not working as intended as the calibration of the sensors did not match the actual conditions in space. These problems were addressed by recalibrating the sensors in-orbit. The work was done by comparing the sensor results with each other and with an independent attitude estimation based on the ESTCube-1 camera.

3.1 Analysing Sun sensor measurements and filtering

The Sun sensors were calibrated beforehand to calculate a Sun vector based on the voltage results from the sensors. However, this approach was unsuccessful. The possible causes for this are:

- During the calibration process both PSD-s were only calibrated in one dimension and the differences based on the produced current were not taken into account.
- Temperature influences that are not accounted for.
- The vibrations of the launch could have caused the sensor to move in relation to the mask of the Sun sensor.

The reference voltages directly affect the Sun vector calculation and are especially important when the edge of the satellite is towards the Sun, because the sensors provide a weaker signal and the error in the reference voltage affects the results more. Instead of the calibration, the equation given in the PSD datasheet to calculate the angle of incidence was used. One of the six Sun sensors is also not working, but this is not critical as the UKF is able to also estimate attitude when the Sun vector is not present. This functionality was originally developed to account for the eclipse.

Because we were not able to use calibration data, the results of the Sun vector calculation were inaccurate when the edge of the satellite was towards the Sun. This meant that to get a better attitude estimation the FOV of the Sun sensors is limited to $\pm$ 36.7° instead of the original $\pm$ 45°. Due to the growing error the covariance for the Sun vector is also changed in the UKF. When the Sun direction is within $\pm$ 20°, the covariance is set to 1.75×10^{-6}, but when the sun direction changes towards the edge of the satellite the covariance matrix elements are quadratically increased up to 0.01. The used covariances are based on the performance of attitude determination with different covariances. A filtered Sun vector is presented in Figure 4. When the sun vector is not calculated due to the FOV, it is set to zero.

3.2 Angular velocity and Sun vector validation

After being able to calculate the Sun vector, it was possible to validate the results of both the Sun sensors and gyroscopes. This was done by extrapolating the Sun vector provided by the Sun sensor with the angular velocity measured by

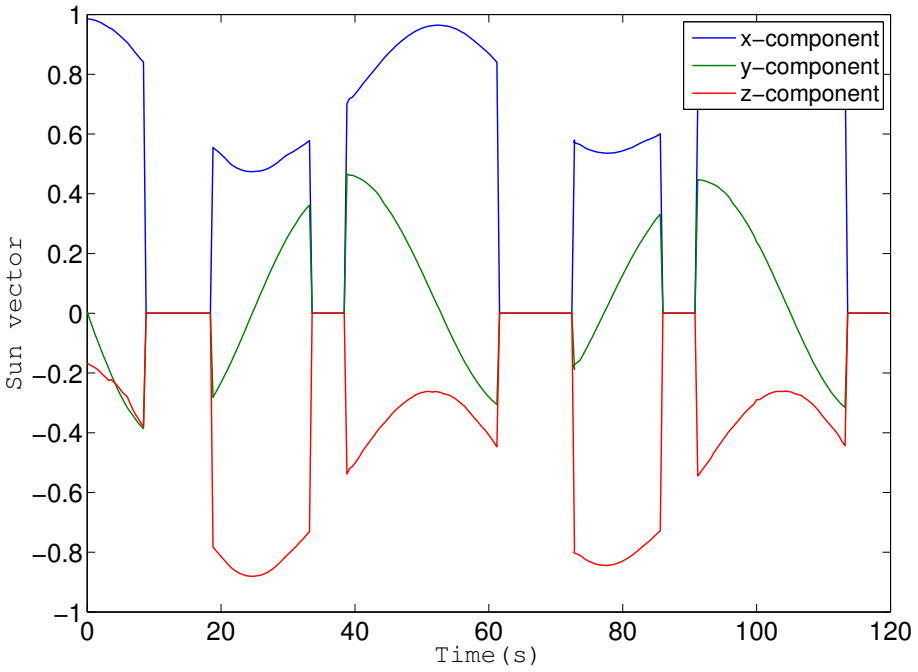

Figure 4: A typical Sun sensor measurement sample.

the gyroscopes. The extrapolated vector was then compared to the actual measurements to validate the results. The gyroscope biases were then improved by making the extrapolated vector and actual measurement match up as closely as possible. Because over many rotations the Sun vector that is calculated when the Sun is perpendicular to a certain side is rather accurate and the time difference is also very accurate then this method is more accurate then the calibration which was made in lab. The setup in the lab included a test bench with a high uncertainty and no temperature information was recorded [2]. As this comparison was done to improve functionality, no accuracy estimation for the process was done. The extrapolated and measured Sun vector plots are presented in Figure 5. On the plot it is possible to see the measured and extrapolated Sun vector 750 seconds to 900 seconds after the start of the extrapolation and the estimated and the measured Sun vectors are still very well aligned.

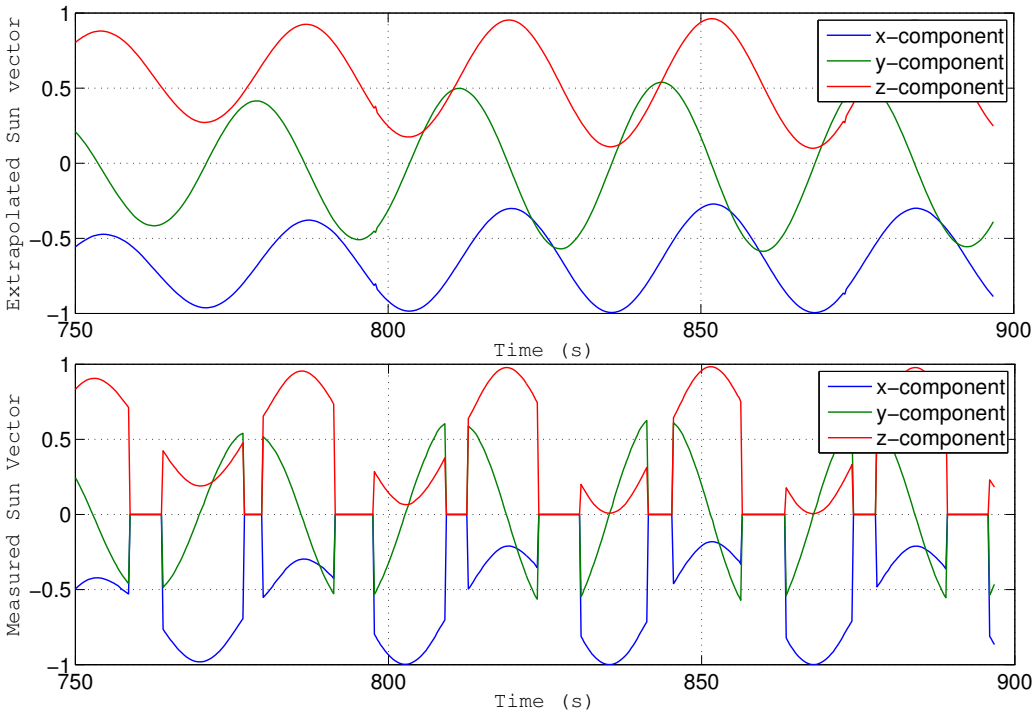

Figure 5: Extrapolated Sun vector compared to the measured Sun vector

3.3 Magnetometer bias estimation

ESTCube-1 has ferromagnetic materials on-board that resulted in a residual magnetic moment which affected both attitude control and attitude determination. The magnetic moment induced additional biases to the magnetometers that needed to be removed before the satellite was able to calculate the Earth's magnetic field vector. This is done by comparing the magnetic field vector with the combined results of the Sun vector, angular velocity and also previous vector measurements. The process is performed by the Kalman filter which is able to estimate the difference between the actual magnetic field and the measured magnetic field. Then the calculated bias is removed and another attitude determination simulation run with the new magnetic field input. After a few iterations the difference between the fields stops getting smaller. After this process both the Sun vector data and the magnetic field data match the respective estimated fields. This means that the magnetometers are then also able to provide a magnetic field estimation that

works together with the rest of the attitude determination. Due to the methodology of sensor calibration, the uncertainty of the system needs to be estimated by comparing it to an independent attitude source, this was done as described in Chapter 4. The results of the bias correction are presented in the Figure 6

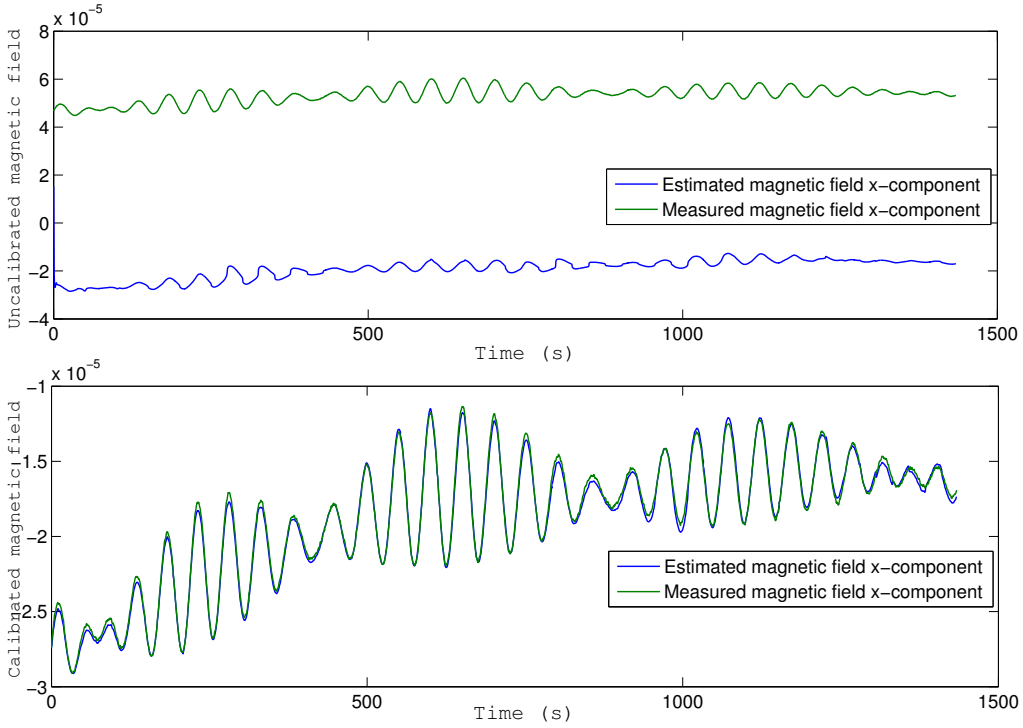

Figure 6: Magnetic field measurements with and without the bias correction

3.4 Temperature calibration of magnetometers and gyroscopes

By analysing the data over a period of a few orbits, a correlation between temperature and the difference between the estimated and calculated magnetic field was identified. The temperature sensors near the magnetometers and gyroscopes were used to fit a function to compensate for temperature changes over an orbit. This function changed both the offsets and gain for different axes for magnetometers and gyroscopes. For magnetometers, a second order polynomial was used for gains and offsets. For the gyroscopes, a polynomial function that removes the offsets based on temperature was used, the gains were not dependent on the

temperature significantly. Thermal calibration of the Sun sensors was not possible because there are no temperature sensors that are able to accurately estimate the temperature of the side panels of the satellite. The difference between the estimated and actual magnetic field before and after temperature calibration is presented in the Figure 7. This plot shows the temperature range from 3.5° to 26°, which is the temperature range over an orbit for the ADCS sensors.

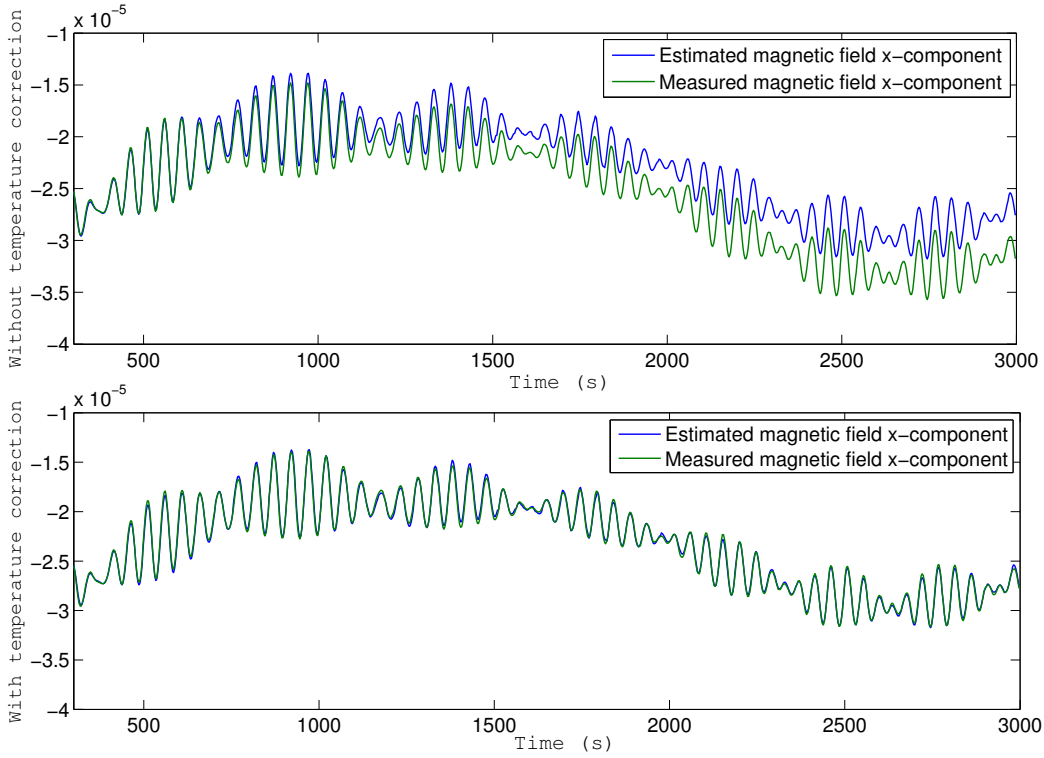

Figure 7: Magnetic field measurements with and without the temperature calibration

3.5 Improving the inertia matrix estimation and implementation

The inertia matrix for the satellite was estimated from the computer-aided design (CAD) model, which included all of the components of the satellite. This model was used in simulations, attitude determination and attitude control. However after launching up the satellite it was possible to see from the uncontrolled

rotation of the satellite that the stable principal axes of rotation estimated from the inertia matrix did not match up with the actual behaviour in orbit. This meant that a more realistic inertia matrix had to be estimated, that would match the uncontrolled rotation. Both the attitude control and determination use the inertia matrix because they are based on the Euler's rotation equations.

For the simulations, the influence from the residual magnetic moment was accounted for and an inertia matrix that would behave the same way in simulations was estimated. This was done by varying the numbers manually, because it wasn't possible to estimate it analytically and writing a program that would minimize the error would have taken a longer time. The inertia matrix estimations were not important at lower speeds where most of the calibration of the system was done, but it became more important when increasing the angular velocity over 50 deg·s^{-1}. This approach was further verified, when it minimized the noise in the attitude determination output at higher angular velocities and improved the speed at which the satellite would spin up using the spin controller. This result will be presented in an upcoming study of the attitude control system written by the author of this thesis.

After improving the inertia matrix the Kalman filter was also improved by changing the propagation to include the full inertia matrix instead of only the diagonal elements. This was also done to improve the performance of the filter at higher angular velocities. The resulting improved inertia matrix, I.

$$\boldsymbol{I} = \begin{pmatrix} 0.0019986 & 4.0097 \cdot 10^{-5} & 5.3287 \cdot 10^{-5} \\ 4.0097 \cdot 10^{-5} & 0.0021620 & 1.9806 \cdot 10^{-5} \\ 5.3287 \cdot 10^{-5} & 1.9181 \cdot 10^{-5} & 0.0022451 \end{pmatrix}$$

In addition to taking the residual magnetic moment into account when simulating the uncontrolled behaviour of the satellite, the torque caused by the residual magnetic moment of the satellite was included in the torque calculations for the Kalman filter. This was done to improve the propagation step in the filter to further improve performance at high angular velocities.

3.6 Improving the measurement noise covariance matrix and model noise matrix for Kalman filter

First, the measurement noise covariance matrix was improved by analysing the results based on a few images and manually editing the covariance matrix. Then the covariances were further changed with additional images analysed. Additional varying covariances were implemented so that the Kalman filter would consider the angular velocity more accurate compared to other sensors at very high angular velocities.This was done to reduce the impact of timing issues when taking the sensor measurements.The covariance was changed linearly from $6 \cdot 10^{-6}$ rad·s^{-1} to $0.6 \cdot 10^{-6}$ rad·s^{-1} for angular velocities from 0 to 360 deg·s^{-1}. This made the attitude output of the system less noisy at higher angular speeds.

To estimate a more accurate model noise covariance matrix a series of simulations were run that compared a set of 15 images to the attitude determined by the Kalman filter while changing the four model noise matrix elements. Each element was varied to an order of magnitude higher and lower that resulted in 81 total simulations. The first element changed represents the expected noise in the kinematic equations, the next element the expected noise in the dynamic equations and the final two elements the expected noise in sensor bias states [8]. Because there existed a lot of local minimums in this process, making an additional simulation around a local minimum was not performed, but the most accurate local minimum was chosen for further attitude estimations.

The resulting model noise covariance matrix, Q, and the measurement noise covariance matrix, R.

$$\boldsymbol{Q} = \begin{pmatrix} 1.75 \cdot 10^{-6} & 1.75 \cdot 10^{-6} & 1.75 \cdot 10^{-6} \\ 2.4 \cdot 10^{-7} & 2.4 \cdot 10^{-7} & 2.4 \cdot 10^{-7} \\ 6 \cdot 10^{-6} & 6 \cdot 10^{-6} & 6 \cdot 10^{-6} \end{pmatrix}$$

$$\boldsymbol{R} = \begin{pmatrix} 1 \cdot 10^{-6} & 1 \cdot 10^{-6} & 1 \cdot 10^{-6} \\ 1 \cdot 10^{-2} & 1 \cdot 10^{-2} & 1 \cdot 10^{-2} \\ 1 \cdot 10^{-4} & 1 \cdot 10^{-4} & 1 \cdot 10^{-4} \\ 1 \cdot 10^{-5} & 1 \cdot 10^{-5} & 1 \cdot 10^{-5} \end{pmatrix}$$

4 Attitude determination system performance

During the characterisation of the system, the focus was on the functionality of attitude determination and accuracy estimations were overlooked to concentrate on improving the system overall. For calibration, sensor measurements were used to estimate the biases for other sensors. Due to this, the uncertainty of the system became impossible to estimate and validate without a reference for the attitude. This was solved by comparing the attitude determination results of the ADCS with image-based attitude estimation and calculating the uncertainty budgets for both methods.

4.1 Uncertainty estimation for the attitude determination system

The uncertainty for the ADS is based on the uncertainty estimations of the sensors, the different models used for attitude determination, the uncertainty of the moment of inertia and time uncertainty on-board. The expanded uncertainty of the attitude determination system of 1.52° is presented in Table 1. A detailed uncertainty analysis is also presented in a separate study [1].

δu_{STD}^{ADS} is the uncertainty contribution by the ADS sensors estimated using a simulation of attitude determination for the part of the orbit where most of the images are taken. This uncertainty is based on a separate study by Slavinskis et al [2].

Another contributor is the geomagnetic field model uncertainty δu_{Mag}^{ADS}. This represents the uncertainty caused by the IGRF 11 model, which is 26 nY/Year, which in total is 105 nT in our case[33].

The two contributors, δu_{Nut}^{ADS} and δu_{Prec}^{ADS} represent the uncertainty of Earth's precession and nutation models used in calculations. The uncertainty estimations are based on a fixed point where the Earth-centered inertial frame and Earth-centered Earth-fixed frame were equal in 1997 [8, p. 65]. The precession of the Earth's rotation axis is 50 s of arc per year and the nutation 9.2 s of arc per 19 years [7, p. 27] The rotation model is used by the geomagnetic field model, which means the rotation uncertainty contributes to the total uncertainty of the attitude

determination.

δu_{Pos}^{ADS} is the uncertainty of position caused by the (SGP4) implementation. The position uncertainty when the two-line elements (TLE) are up-to-date is up to 6 km [34].

The Sun direction model, δu_{Sun}^{ADS}, contributes to the uncertainty, because the measured Sun vector is compared against it. The accuracy of the Sun model is 1 arcminute [26, p. 39].

Quantity	Standard uncertainty	Probability distribution	Uncertainty contribution, deg
δu_{STD}^{ADS}	0.6°	Normal	0.6°
δu_{Mag}^{ADS}	105 nT	Normal	0.42°
δu_{Prec}^{ADS}	0.15°	Rectangular	0.15°
δu_{Pos}^{ADS}	3.5 km	Rectangular	0.1°
δu_{Sun}^{ADS}	0.01°	Rectangular	0.01°
δu_{Nut}^{ADS}	0.0015°	Rectangular	0.0015°
Combined standard uncertainty			0.76°
δU^{ADS}, expanded uncertainty (95% confidence level, k=2)			1.52°

Table 1: Uncertainty budget for ADS [1]

4.2 Uncertainty estimation for image-based attitude determination

To provide an estimation for the uncertainty of the attitude determination we also need to characterise the image-based attitud determination. We take into account the limitations of the camera on-board ESTCube-1 and the method used for estimating the attitude from images [32]. Table 2 presents the uncertainty budget of image-based attitude determination. The analysis was also presented in a study that characterises the attitude determination system [1].

δu_{Sel}^{Cam} is the uncertainty caused by the manual selection of points on the image and finding the respective point on a geographic coordinate system. This is estimated from the angles between the coordiantes on the image and the geographical coordinates after matching them up to the best of our abilities.

δu_{Time}^{Cam} is the inherent uncertainty of time. This comes from the inability to determine the accuracy of time between the CDHS and the CAM subsystems. While the time was synced with ground to provide the best results, some uncertainty still remained. Additional measures were taken to remove some of the time uncertainty, which are described under comparison results.

The camera resolution uncertainty, δu_{Res}^{Cam}, directly affects how accurate the process is, because anything under 1 pixel can not be distinguished. This also includes the specific shapes and locations of landmarks that were used to match the images with geographic points [32].

δu_{Lens}^{Cam} is caused by the simplification of the barrel distortion model, which is used to remove the distortion caused by the lens and the optics of the camera.

Quantity	Standard uncertainty	Probability distribution	Uncertainty contribution, deg
δu_{Sel}^{Cam}	0.37°	Rectangular	0.37°
δu_{Time}^{Cam}	29 ms	Rectangular	0.21°
δu_{Res}^{Cam}	0.04°	Rectangular	0.04°
δu_{Lens}^{Cam}	0.02°	Rectangular	0.02°
Combined standard uncertainty			0.43°
δU^{Cam}, expanded uncertainty (95% confidence level, k=2)			0.86°

Table 2: Uncertainty budget of image-based attitude determination. [1]

4.3 Comparison results

To validate the ADS of ESTCube-1 the results from two independent attitude determination methods were compared to each other. The images for this comparison are chosen so that the uncertainty would be minimized. This included choosing images from areas around the equator because we were able to capture the most landmass from those regions. Because the satellite had a residual magnetic moment caused by ferromagnetic materials, the satellite followed the Earth's magnetic field when orbiting, which meant that only certain areas were imaged reliably. Most of the images are from Africa, because it is easier to detect landmarks in deserts compared to other terrains. An image over Africa was also presented as a sample image in Chapter 2.

The uncertainty was estimated at a certain part in orbit, but the uncertainty of attitude estimation varies during the orbit. However, the uncertainty budget was relevant for the E-sail mission, because the uncertainty in the parts of the orbit where the experiment is run is lower than in the part where the images are taken [2]. The attitude determination performs a lot worse in eclipse and also worse when the Sun direction is close to parallel with the magnetic field vector.

When taking the images we aimed to take many of them in a row. This was beneficial to reduce the uncertainty of time, because the relative time between the images is very well known. The smallest difference between the ADS attitude and image-based attitude is estimated in a 3 second window. However, the relative time difference between the images had to be the known amount. This prevented the overestimation of the accuracy when doing the comparison, but also limited us to using only sets of images.

The uncertainty budgets are valid for spin rates up to 7.1 $\text{deg}\cdot\text{s}^{-1}$because that is the speed where the sensor calibration is made and higher spin rates increase the time uncertainty contribution towards image-based attitude determination. It can also make the Kalman filter perform worse, because it is harder to accurately predict the next step at higher spin rates. Higher angular speeds were not used to calibrate because it is considerably harder to determine attitude from images due to the blurring of the image. For the E-Sail mission the spin rates are around 20 $\text{deg}\cdot\text{s}^{-1}$, for which the validation process will give a good estimation for [6].

The validation process included 15 images. All the samples have differences of less than 1.44° between the attitude estimations which is within the expanded uncertainty of comparison (95% confidence level, k=2) of 1.75°. The combined uncertainty is defined by the equation

$$\delta U = \sqrt{\left(\delta U^{ADS}\right)^2 + \left(\delta U^{Cam}\right)^2} = 1.75^\circ.$$

The results are described in detail in Table 3. After the calibration of the system the system was able to achieve the required attitude determination accuracy of 2° [2].

Sample	1	2	3	4	5
Difference, deg	0.31	0.63	1.26	0.7	1.16
Sample	6	7	8	9	10
Difference, deg	1.32	1.43	0.17	1.14	0.45
Sample	11	12	13	14	15
Difference, deg	0.78	0.32	0.18	0.31	0.42

Table 3: Difference between on-board and image-based attitude. [1]

5 Discussions, conclusions and further work

The work presented in this thesis was successful in calibrating the ADS to determine the attitude with the required accuracy of 2°. This was achieved by calibrating the sensors and improving the parameters and implementation of the Kalman filter. For Sun sensors a low-level filtering system was implemented. For gyroscopes the offsets were adjusted to match the Sun vector data and temperature calibration was performed. For magnetometers the bias was estimated based on the Kalman filter output and temperature calibration was performed. The inertia matrix estimation was improved and the full inertia matrix was implemented into attitude control and determination instead of only the diagonal components. The model noise matrix and the sensor covariances were matched with the calibrated sensors.

After this process the sensors were validated by comparing the attitude determination with image-based attitude estimation. Uncertainty budgets for both the ADS and image-based attitude determination were estimated. The combined uncertainty of the comparison was 1.75° and the highest difference between the two attitude determination methods was 1.44° from a set of 15 images.

At speed up to 100 deg·s^{-1} the system performed as expected, but at higher speed the Kalman filter was unable to recover from the situation where the Sun vector and Magnetic field vector were very closely aligned to each other. The drift from that situation was considered as bias by the filter. This problem could have been solved by additional fault-checking mechanism or varying covariances, but this was not deemed necessary as attitude information was not used to spin up to speeds above 100 deg·s^{-1}. The magnetic field and angular velocity measurements were used to perform spin-up to an angular rate higher than 2 revolutions per second, which is the highest known controlled spin rate for nanosatellites.

Also a small improvement for the calibration was recently conceived, but not implemented. The image-based attitude could have been improved if the angular velocity was taken into account when the image was corrected for distortions. The imaging process starts by filling the pixels on top of the image first and when the satellite is rotating the bottom part of the image will be shifted towards the rotation. This method could be useful if a similar method was used to validate

the attitude determination system at higher angular velocities and to get a better accuracy for the overall estimation.

By characterising the ADS we learned a lot about the performance of different sensors in space. Laboratory tests were unable to fully imitate the conditions in orbit and methods to calibrate the sensors and upload new software to the satellite are incredibly useful in nanosatellite missions. Different sensors and duplicating sensors are used for both risk mitigation and improving the measurement accuracy. To improve the Sun sensor design further a temperature sensor should be included and the reference voltage also measured. The FOV should also be improved to be able to cover every possible Sun vector even when the sensors are not performing optimally. The lessons learned from the ADS of ESTCube-1 will be used in the future missions of the ESTCube project, which is currently in development and will include an improved design of the Sun sensors and a Star sensor. More focus will be on the magnetic influences of different materials and also on a better estimation of the inertia matrix. The lessons learned for ESTCube-1, which will include the lessons learned for the ADS, will be presented in a separate article by A. Slavinskis, et.al.

ESTCube-1 in-orbit attitude determination validation

Hendrik Ehrpais

Summary

The aim of this Bachelor thesis was to validate the attitude determination system for the ESTCube-1 satellite. After launching the satellite into space, a series of problems with the sensors and the attitude determination process were encountered. This work describes how these problems were overcome and hpw the system was calibrated to achieve an attitude determination capability that is able to estimate the attitude with an uncertainty below 2 degrees. This was the requirement set by the ESTCube-1 mission on attitude determination accuracy.

A review on the attitude determination processes for different nano- and microsatellites is presented. The system design for ESTCube-1 attitude determination system is also presented. This involves the description of the Sun sensors, magnetometers and gyroscopes, an overview of the Unscented Kalman filter and also describes the image based attitude determination.

In-orbit characterisation is presented in detail with the steps taken to overcome problems that the attitude determination faced. The calibration for Sun sensors performed on ground was not working and a separate way to estimate the angle of incidence had to be developed. This was based on the equation given in the position sensitive device datasheet used in the Sun sensors. A filter was developed that reduced the effective field of view for the Sun sensors. The gyroscope offsets were recalculated and the angular velocity measurements and Sun vector measurements were validated by comparing them to each other. Using the Unscented Kalman filter we were able to estimate the effect of the residual magnetic moment on the magnetometer biases. The biases were then removed and the functionality to measure the Earth's magnetic field with magnetometers was achieved. Also a temperature calibration for magnetometers and gyroscopes was developed based on the data from the satellite in orbit. Also the inertia matrix estimation was improved based on the uncontrolled behaviour of the satellite and making the satellite behave in the simulations the same way as it does in space. All of the elements of the inertia matrix were used instead of only the diagonal elements to

provide a more accurate attitude estimation at higher angular velocities (over 50 $\mathrm{deg \cdot s^{-1}}$). Furthermore, the measurement noise covariance matrix and the model noise matrix for Kalman filter were improved based on the comparison of the attitude determination system with the image-based attitude determination.

The uncertainty budgets for both the attitude determination system and the image-based attitude determination system were developed. The combined uncertainty for the comparison between the image-based attitude and attitude determination system was estimated. This comparison was used to validate the attitude determination system. The comparison at the specific conditions that the images were taken at gave us an estimation for the functionality of our ADS. Based on a set of 15 images, the maximum error between the two methods of attitude determination was 1.44°, which is withing the 2 degrees that was required for the ESTCube-1 mission. This means the calibration process was successful in making the attitude determination system functional.

The lessons learned from the in-orbit validation will be used in developing the upcoming ADCS for the next ESTCube missions, where the author will also take active part in. For example, a new Sun sensor design is being developed and star trackers will be used for the ADCS on the next ESTCube satellite.

ESTCube-1 asendi määramise ja kontrolli süsteemi valideerimine orbiidil

Hendrik Ehrpais

Kokkuvõte

Selle bakalaureuse töö eesmärk oli valideerida ESTCube-1 asendi määramise alamsüsteemi töö. Peale satelliidi saatmist kosmosesse, esinesid probleemid asendi määramise süsteemi anduritega ja asendi määramise protsessiga. See töö kirjeldab, kuidas nendest probleemidest lahti saadi ning kuidas asendi määramise süsteemi kalibreeriti. Eesmärgiks oli saavutada asendi määramise täpsus, mille määramatus oleks alla 2 kraadi. See nõue oli seatud ESTCube-1 missiooni poolt.

Töös esitatakse ka ülevaade erinevate nano- ja mikrosatelliitide asendi määramise süsteemidest. Kirjeldatakse detailsemalt ESTCube-1 asendi määramise süsteemi. Tuuakse välja päikeseandurite, magnetomeetrite ja güroskoopide kirjeldus ning esitatakse kasutatud Kalmani filtri tööpõhimõte. Lisaks kirjeldatakse pildilt asendi määramise protsessi, mille kaudu valideeriti asendi määramise süsteemi tulemused.

Kirjeldatakse süsteemi karakteriseerimist ning viise, kuidas lahendati probleeme, mis tekkis asendi määramise süsteemi kasutamisel kosmoses. Päikesesandurite Maa peal tehtud kalibratsioon ei töödanud orbiidil. Selle tõttu oli vaja välja töötada optilise positsiooni anduri spetsifikatsioonides leitava valemi põhjal viis, kuidas kõige paremini määrata päikese vektor. Et saada paremaid tulemusi asendi määramisel, filtreeritakse osa päikese vektori tulemustest välja. Selle põhjuseks on, et kui satelliidi äär on Päikese suunas, siis tulemuste määramatus läheb väga suureks. Güroskoopide tulemuste kõrvalekalde hindamiseks kasutati päikeseandurite tulemusi. Seejärel kasutati päikeseandureid, et kalibreerida güroskoobid. Kasutades Kalmani filtrit ennustati magnetomeetrite kõrvalekalded, mis olid põhjustatud jääkmagnetmomendi poolt. Selle abil suutsime kalibreerida magnetomeetrid nii, et oli võimalik Maa magnetvälja mõõta. Seejärel moodustati funktsioonid temperatuuriandurite andmete põhjal, mis võimaldasid korrigeerida nii magnetomeetrite kui ka güroskoopide tulemusi. Lisaks kasutati simulatsioone, et leida parem hinnang inertsimaatriksile, mis oli algselt tehtud satelliidi arvutimudeli põhjal. Inertsimaatriks saadi satelliidi pöörelmise simulatsioonide kokku viimisel kontrollimata pöörlemise andmetega orbiidilt. Selle protsessi eesmärk

oli, et asendi määramine töötaks paremini kõrgematel pöörlemiskiirusel(üle 50 kraadi sekundis). Veel hinnati piltide abil Kalman filtri parameetrite väärtusi. Seda tehti võrreldes piltide abil asendi määramist asendi määramise süsteemiga satelliidil erinevate parameetrite korral.

Et hinnata asendi määramise süsteemi täpsust, hinnati nii asendi määramise süsteemi kui ka pildi abil asendi määramise määramatused. Selle võrdluse koondmääaramatust kasutati, et hinnata, kas satelliidi asendimääramise süsteem vastab nõuetele. Võrdluse käigus kasutati 15 pilti, mis olid tehtud sarnastel tingimustel, et hinnata viga kahe asendi määramise meetodi vahel. Maksimaalne viga sellel võrdlusel oli 1.44°, mis jääb alla 2°määramatuse nõudele. Selle tõttu võib lugeda kalibreerimist edukaks.

Asendi määramise valideerimise protsessi õppetunde kasutatakse järgmiste asendi määramise süsteemide disainimisel ESTCube projekti jaoks. Seal kavatseb ka töö autor tulevikus järgmiste projektide kallal töötada. Näiteks kasutatakse neid õppetunde juba, et disainida uusi päikeseandureid ning oleme otsustanud kasutada täheandureid järgmistel ESTCube satelliitidel.

6 Acknowledgements

I would like to express my gratitude to fellow team members from ESTCube-1, especially Andris Slavinskis, Henri Kuuste, Erik Kulu, Indrek Sünter, Jaan Viru who worked with me on the in-orbit attitude determination characterisation and calibration.I would also like to thank the Danish AAUSAT CubeSat team for kindly providing the base for simulations and attitude determination.

7 References

[1] A. Slavinskis, H. Ehrpais, H. Kuuste, I. Sünter, J. Viru, E. Kulu, J. Kütt, and M. Noorma, "Flight results of ESTCube-1 attitude determination system," Journal of Aerospace Engineering (2015).

[2] A. Slavinskis, E. Kulu, J. Viru, R. Valner, H. Ehrpais, T. Uiboupin, M. Järve, E. Soolo, J. Envall, T. Scheffler, I. Sünter, H. Kuuste, U. Kvell, J. Kalde, K. Laizāns, E. Ilbis, T. Eenmäe, R. Vendt, K. Voormansik, I. Ansko, V. Allik, S. Lätt, and M. Noorma, "Attitude determination and control for centrifugal tether deployment on ESTCube-1 nanosatellite," Proc. Estonian Acad. Sci. **63(2S)**, 242–249 (2014).

[3] P. Janhunen and A. Sandroos, "Simulation study of solar wind push on a charged wire: basis of solar wind electric sail propulsion," Ann. Geophys. **25**, 755–767 (2007).

[4] P. Janhunen, P. K. Toivanen, J. Polkko, S. Merikallio, P. Salminen, E. Hæggström, H. Seppänen, R. Kurppa, J. Ukkonen, S. Kiprich, G. Thornell, H. Kratz, L. Richter, O. Krömer, R. Rosta, M. Noorma, J. Envall, S. Lätt, G. Mengali, A. A. Quarta, H. Koivisto, O. Tarvainen, T. Kalvas, J. Kauppinen, A. Nuottajärvi, and A. Obraztsov, "Electric solar wind sail: Toward test missions," Rev. Sci. Instrum. **81**, 111301:1–11 (2010).

[5] S. Lätt, A. Slavinskis, E. Ilbis, U. Kvell, K. Voormansik, E. Kulu, M. Pajusalu, H. Kuuste, I. Sünter, T. Eenmäe, K. Laizāns, K. Zālīte, R. Vendt, J. Piepenbrock, I. Ansko, A. Leitu, A. Vahter, A. Agu, E. Eilonen, E. Soolo, H. Ehrpais, H. Lillmaa, I. Mahhonin, J. Mõttus, J. Viru, J. Kalde, J. Šubitidze, J. Mucenieks, J. Šate, J. Kütt, J. Poļevskis, J. Laks, K. Kivistik, K.-L. Kusmin, K.-G. Kruus, K. Tarbe, K. Tuude, K. Kalniņa, L. Joost, M. Lõoke, M. Järve, M. Vellak, M. Neerot, M. Valgur, M. Pelakauskas, M. Averin, M. Mikkor, M. Veske, O. Scheler, P. Liias, P. Laes, R. Rantsus, R. Soosaar, R. Reinumägi, R. Valner, S. Kurvits, S.-E. Mändmaa, T. Ilves, T. Peet, T. Ani, T. Tilk, T. H. C. Tamm, T. Scheffler, T. Vahter, T. Uiboupin, V. Evard, A. Sisask, L. Kimmel, O. Krömer, R. Rosta, P. Janhunen,

J. Envall, P. Toivanen, T. Rauhala, H. Seppänen, J. Ukkonen, E. Haeggström, R. Kurppa, T. Kalvas, O. Tarvainen, J. Kauppinen, A. Nuottajärvi, H. Koivisto, S. Kiprich, A. Obraztsov, V. Allik, A. Reinart, and M. Noorma, "ESTCube-1 nanosatellite for electric solar wind sail in-orbit technology demonstration," Proc. Estonian Acad. Sci. **63(2S)**, 200–209 (2014).

[6] A. Slavinskis, U. Kvell, E. Kulu, I. Sünter, H. Kuuste, S. Lätt, K. Voormansik, and M. Noorma, "High spin rate magnetic controller for nanosatellites," Acta Astronaut. **95**, 218–226 (2014).

[7] J. R. Wertz, ed., *Spacecraft Attitude Determination and Control* (Kluwer Academic Publishers, 1978). ISBN: 978-9027712042.

[8] K. F. Jensen and K. Vinther, "Attitude determination and control system for AAUSAT3," Master's thesis, Aalborg University (2010).

[9] L. Johnson, M. Whorton, A. Heaton, R. Pinson, G. Laue, and C. Adams, "NanoSail-D: A solar sail demonstration mission," Acta Astronaut. **68**, 571–575 (2011).

[10] T. Svitek., L. Friedman, W. Nye, C. Biddy, and M. Nehrenz, "Voyage continues — LightSail-1 mission by the planetary society," in "61st International Astronautical Congress," , vol. 1 (2010), vol. 1, pp. 802–810. ISBN: 978-161782368-8.

[11] V. Lappas, N. Adeli, L. Visagie, J. Fernandez, T. Theodorou, W. Steyn, and M. Perren, "CubeSail: A low cost CubeSat based solar sail demonstration mission," Adv. Space Res. **48**, 1890–1901 (2011).

[12] J. C. Springmann, A. J. Sloboda, A. T. Klesh, M. W. Bennett, and J. W. Cutler, "The attitude determination system of the RAX satellite," Acta Astronaut. **75**, 120–135 (2012).

[13] N. C. Deschamps, C. C. Grant, D. G.Foisy, R. E. Zee, A. F. Moffat, and W. W. Weiss, "The BRITE space telescope: Using a nanosatellite constellation to measure stellar variability in the most luminous stars," Acta Astronaut. **65**, 643–650 (2009).

[14] O. Koudelka, G.Egger, B. Josseck, N. Deschamp, C. C. Grant, D.Foisy, R. Zee, W.Weiss, R. Kuschnig, A. Scholtz, and W.Keim, "TUGSAT-1/BRITE-Austria — the first Austrian nanosatellite," Acta Astronaut. **64**, 1144–1149 (2009).

[15] M. Borgeaud, N. Scheidegger, M. Noca, G. Roethlisberger, F. Jordan, T. Choueiri, and N. Steiner, *Small Satellite Missions for Earth Observation* (Springer, 2010), chap. SwissCube: The First Entirely-Built Swiss Student Satellite with an Earth Observation Payload, pp. 207–213.

[16] J. A. Larsen, R. Amini, and R. Izadi-Zamanabadi, "Advanced attitude control af pico sized satellites," in "56th International Astronautical Congress," , vol. 5 (2005), vol. 5, pp. 2865–2871. ISBN: 978-1-60423-648-4.

[17] D. E. Rowland, J. Hill, P. Uribe, J. Klenzing, F. Hunsaker, M. Fowle, K. Simms, H. Hancock, M. Saulino, D. Guzman, A. Willingham, A. Weatherwax, J. Kujawski, M. McColgan, R. Carroll, J. Williams, J. DeMatteo, O. Ganel, C. Naegeli, L. Lutz, and C. Dailey, "The NSF Firefly CubeSat mission: Rideshare mission to study energetic electrons produced by lightning," in "IEEE Aerospace Conference," (2011).

[18] A. Kestil, T. Tikka, , P. Peitso, J. Rantanen, A. Näsilä, K. Nordling, H. Saari, R. Vainio, P. Janhunen, J. Praks, and M. Hallikainen, "Aalto-1 nanosatellite — technical description and mission objectives," Geosci. Instrum. Method. Data Syst. **2**, 121–130 (2013).

[19] W. Blackwell, G. Allen, C. Galbraith, T. Hancock, R. Leslie, I. Osaretin, L. Retherford, M. Scarito, C. Semisch, M. Shields, M. Silver, D. Toher, K. Wight, D. Miller, K. Cahoy, and N. Erickson, "Nanosatellites for earth environmental monitoring: The MicroMAS project," in "32nd IEEE International Geoscience and Remote Sensing Symposium," (2012).

[20] J. Dickinson, C. DeForest, and T. Howard, "The CubeSat heliospheric imaging experiment (CHIME)," in "IEEE Aerospace Conference," (2011).

[21] K. Sarda, S. Eagleson, E. Caillibot, C. Grant, D. Kekez, F. Pranajaya, and R. E. Zee, "Canadian advanced nanospace experiment 2: Scientific and technological innovation on a three-kilogram satellite," Acta Astronaut. **59**, 236–245 (2006).

[22] E. H. Peterson, G. Fotopoulos, and R. E. Zee, "A feasibility assessment for low-cost InSAR formation-flying microsatellites," IEEE Trans. Geosci. Remote Sens. **47**, 2847–2858 (2009).

[23] A. Scholz, W. Ley, B. Dachwald, J. Miau, and J. Juang, "Flight results of the COMPASS-1 picosatellite mission," Acta Astronaut. **67**, 1289–1298 (2010).

[24] C. Bridges, S. Kenyon, C. Underwood, and V. Lappas, "STRaND-1: The world's first smartphone nanosatellite," in "2nd International Conference on Space Technology," (2011).

[25] C. C. Finlay, S. Maus, C. D. Beggan, T. N. Bondar, A. Chambodut, T. A. Chernova, A. Chulliat, V. P. Golovkov, B. Hamilton, M. Hamoudi, R. Holme, G. Hulot, W. Kuang, B. Langlais, V. Lesur, F. J. Lowes, H. Lühr, S. Macmillan, M. Mandea, S. McLean, C. Manoj, M. Menvielle, I. Michaelis, N. Olsen, J. Rauberg, M. Rother, T. J. Sabaka, A. Tangborn, L. Tøffner-Clausen, E. Thébault, A. W. P. Thomson, I. W. Z. Wei, and T. I. Zvereva, "International Geomagnetic Reference Field: the eleventh generation," Geophys. J. Int. **183**, 1216–1230 (2010).

[26] O. Montenbruck and T. Pfleger, *Astronomy on the Personal Computer* (Springer-Verlag, 1994), 2nd ed. ISBN: 978-3-540-67221-0.

[27] F. R. Hoots and R. L. Roehrich, "Spacetrack report no. 3 — models for propagation of NORAD element sets," Tech. rep., Peterson AFB: Office of Astrodynamics, Aerospace Defense Center (1980).

[28] "Hamamatsu S3931 product specification," .

[29] "Honeywell HMC5883L product specification," .

[30] "Invensense ITG-3200 product specification," .

[31] K. Vinther, K. F. Jensen, J. A. Larsen, and R. Wiśniewski, "Inexpensive CubeSat attitude estimation using quaternions and Unscented Kalman Filtering," Online journal Automatic Control in Aerospace (2011).

[32] H. Kuuste, T. Eenmäe, V. Allik, A. Agu, R. Vendt, I. Ansko, K. Laizāns, I. Sünter, S. Lätt, and M. Noorma, "Imaging system for nanosatellite proximity operations," Proc. Estonian Acad. Sci. **63(2S)**, 250–257 (2014).

[33] S. Maus, C. Manoj, J. Rauberg, I. Michaelis, and H. Lühr, "NOAA/NGDC candidate models for the 11th generation International Geomagnetic Reference Field and the concurrent release of the 6th generation Pomme magnetic model," Earth Planets Space **62**, 729–735 (2010).

[34] W. Dong and Z. Chang-yin, "An accuracy analysis of the SGP4/SDP4 model," Chinese Astronomy and Astrophysics **34**, 69–76 (2010).

Non-exclusive licence to reproduce thesis and make thesis public

I, Hendrik Ehrpais

1. herewith grant the University of Tartu a free permit (non-exclusive licence) to:

   (a) reproduce, for the purpose of preservation and making available to the public, including for addition to the DSpace digital archives until expiry of the term of validity of the copyright, and

   (b) make available to the public via the web environment of the University of Tartu, including via the DSpace digital archives until expiry of the term of validity of the copyright,

   ESTCube-1 in-orbit attitude determination validation,

   supervised by Andris Slavinskis and Henri Kuuste,

2. I am aware of the fact that the author retains these rights.

3. I certify that granting the non-exclusive licence does not infringe the intellectual property rights or rights arising from the Personal Data Protection Act.

Tartu, May 26, 2015